

# UAV Formation Optimization for Communication-assisted InSAR Sensing

Mohamed-Amine Lahmeri\*, Víctor Mustieles-Pérez\*<sup>†</sup>, Martin Vossiek\*, Gerhard Krieger\*<sup>†</sup>,  
and Robert Schober\*

\*Friedrich-Alexander-Universität Erlangen-Nürnberg, Germany

<sup>†</sup>German Aerospace Center (DLR), Microwaves and Radar Institute, Weßling, Germany

## Abstract

Interferometric synthetic aperture radar (InSAR) is an increasingly important remote sensing technique that enables three-dimensional (3D) sensing applications such as the generation of accurate digital elevation models (DEMs). In this paper, we investigate the joint formation and communication resource allocation optimization for a system comprising two unmanned aerial vehicles (UAVs) to perform InSAR sensing and to transfer the acquired data to the ground. To this end, we adopt as sensing performance metrics the interferometric coherence, i.e., the local correlation between the two co-registered UAV radar images, and the height of ambiguity (HoA), which together are a measure for the accuracy with which the InSAR system can estimate the height of ground objects. In addition, an analytical expression for the coverage of the considered InSAR sensing system is derived. Our objective is to maximize the InSAR coverage while satisfying all relevant InSAR-specific sensing and communication performance metrics. To tackle the non-convexity of the formulated optimization problem, we employ alternating optimization (AO) techniques combined with successive convex approximation (SCA). Our simulation results reveal that the resulting resource allocation algorithm outperforms two benchmark schemes in terms of InSAR coverage, while satisfying all sensing and real-time communication requirements. Furthermore, we highlight the importance of efficient communication resource allocation in facilitating real-time sensing and unveil the trade-off between InSAR height estimation accuracy and coverage.

## I. INTRODUCTION

The widespread use of unmanned aerial vehicles (UAVs) has revolutionized modern technology, impacting fields like remote sensing, communication, and disaster monitoring [1]. Their versatility and cost-effectiveness have made them an indispensable tool for these diverse applications. Specifically, UAVs excel

in remote sensing applications due to their remarkable ability to swiftly acquire high-quality data, be it for ranging and detection or imaging purposes [2]. In this context, seamless UAV-to-UAV as well as UAV-to-ground connectivity enables the timely collection and transfer of essential information in highly dynamic scenarios. In fact, researchers have made significant strides in developing robust communication architectures that can ensure real-time UAV-based communication even in challenging environments [3].

Interferometric synthetic aperture radar (InSAR) is a well-established remote sensing technique, for which the use of UAVs will open up new application opportunities for the high-resolution observation of small-scale areas and the systematic monitoring of local processes [4]. InSAR systems employ two synthetic aperture radar (SAR) sensors to illuminate a given area from different angles and by analyzing the phase difference of the two received radar signals, information about the topography and temporal variations of the target area can be derived [5]. For InSAR, the sensing area is defined by the region where the ground footprints of the two side-looking radar antennas overlap. Furthermore, conventional sensing performance metrics, such as the detection probability and the false alarm rate, are inadequate for evaluating the InSAR performance. In fact, the key performance metric for estimating interferometric performance is coherence, which is a function of the correlation between the co-registered master and slave SAR images [5]. Another relevant performance metric is the height of ambiguity (HoA), which is a proportionality constant between the interferometric phase and the terrain height and is thus related to the sensitivity of the radar to the ground topography [5]. An interesting trade-off in performance arises here; while a large inter-UAV separation distance leads to a small HoA, improving sensing accuracy, it also leads to a degradation of the image coherence [6]. Based on the above discussion, existing results for conventional UAV-based sensing [7] are not applicable for UAV-based InSAR sensing. Moreover, while some preliminary UAV-based InSAR experiments have been reported in [8], [9], the optimization-based design of these systems has not been yet considered in the open literature.

In this paper, we present the first optimization framework for communication-assisted UAV-based bistatic InSAR sensing. Our contributions can be summarized as follows:

- We adopt InSAR-specific sensing performance metrics such as InSAR coverage, HoA, and interferometric coherence for optimization of InSAR systems.
- We formulate and solve a joint formation and communication resource optimization problem to maximize the UAVs' coverage while guaranteeing the pertinent sensing and communication constraints.
- Our simulations reveal that, in comparison with two benchmark schemes, a significantly larger ground area can be covered with the proposed scheme and highlight interesting InSAR-specific performance trade-offs.

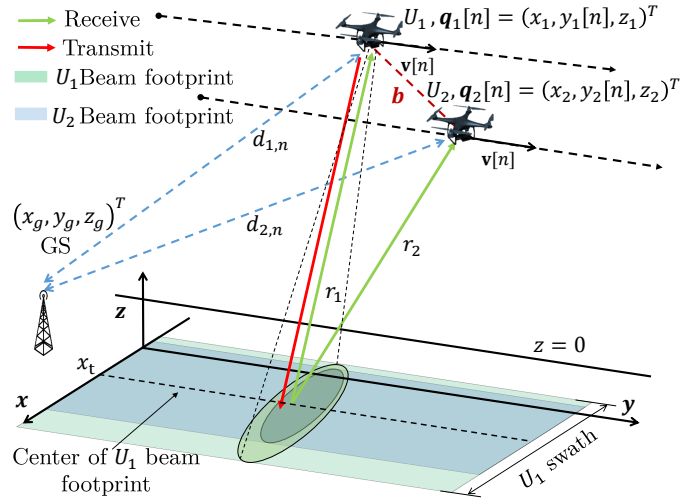


Fig. 1: InSAR sensing system with two UAV SAR sensors and a GS for real-time data offloading.

*Notations:* In this paper, lower-case letters  $x$  refer to scalar numbers, while boldface lower-case letters  $\mathbf{x}$  denote vectors.  $\{a, \dots, b\}$  denotes the set of all integers between  $a$  and  $b$ .  $|\cdot|$  denotes the absolute value operator.  $\mathbb{R}^N$  represents the set of all  $N$ -dimensional vectors with real-valued entries. For a vector  $\mathbf{x} \in \mathbb{R}^N$ ,  $\|\mathbf{x}\|_2$  denotes the Euclidean norm, whereas  $\mathbf{x}^T$  stands for the transpose of  $\mathbf{x}$ . For a real-valued multivariate function  $f(\mathbf{x})$ ,  $\nabla_{\mathbf{x}}f(\mathbf{a})$  denotes the gradient vector of  $f$  with respect to (w.r.t.)  $\mathbf{x}$  evaluated for an arbitrary vector  $\mathbf{a}$ . For real numbers  $a$  and  $b$ ,  $\max(a, b)$  and  $\min(a, b)$  stand for the maximum and minimum of  $a$  and  $b$ , respectively. For a scalar  $x \in \mathbb{R}$ ,  $[x]^+$  refers to  $\max(0, x)$ . The notation  $X_n(\mathbf{x}_1, \dots, \mathbf{x}_i)$  is an equivalent notation for  $X$  highlighting that  $X$  depends on optimization variables  $(\mathbf{x}_1, \dots, \mathbf{x}_i)$  and time slot  $n$ .

## II. SYSTEM MODEL

We consider two rotary-wing UAVs, denoted by  $U_1$  and  $U_2$ , that perform InSAR sensing of a given ground area.  $U_1$ , serving as the master drone, transmits and receives radar signals, whereas  $U_2$ , serving as the slave drone, only receives the echoes. We adopt a three-dimensional (3D) coordinate system, where the  $x$ -axis represents the ground range direction, the  $y$ -axis represents the azimuth direction, and the  $z$ -axis defines the altitude of the drones above ground, see Figure 1. We discretize the total mission time  $T$  into  $N$  uniform time slots  $\delta_t$  such that  $T = N \cdot \delta_t$ . We perform across-track interferometry [4], where both drones are located in the same  $x-z$  plane, also referred to as the across-track plane [4], and follow a linear trajectory, i.e., the stripmap SAR imaging mode is employed [10]. Therefore, the radar coverage along the  $x$ -axis, referred to as swath, is centered w.r.t. a line that is parallel to the  $y$ -axis and passes through point  $(x_t, 0, 0)$ , see Figure 1. Usually, multiple swaths are required to cover a large area, therefore maximizing the

swath is required [11]. Moreover, for InSAR, to ensure that  $U_1$  and  $U_2$  are always in the same across-track plane, they fly with the same fixed velocity  $\mathbf{v}_y = (v_y[1], \dots, v_y[N])^T \in \mathbb{R}^N$  such that in time slot  $n$ , the velocity vector is given by  $\mathbf{v}[n] = (0, v_y[n], 0)^T \in \mathbb{R}^3, \forall n$ , [12]. The location of  $U_i$  in time slot  $n$  is denoted by  $\mathbf{q}_i[n] = (x_i, y[n], z_i)^T, i \in \{1, 2\}$ , where the  $y$ -axis position vector  $\mathbf{y} = (y[1] = 0, y[2], \dots, y[N])^T \in \mathbb{R}^N$  is given by:

$$y[n+1] = y[n] + v_y[n]\delta_t, \forall n \in \{1, N-1\}. \quad (1)$$

Hereinafter, as the  $y$ -axis position is pre-determined, we use the simplified notation  $\mathbf{q}_i = (x_i, z_i)^T \in \mathbb{R}^2, \forall i \in \{1, 2\}$ , to denote the position of  $U_i$  in the across-track plane. Furthermore, the interferometric baseline, which is the distance between the two InSAR sensors, is given by:

$$b(\mathbf{q}_1, \mathbf{q}_2) = \|\mathbf{q}_2 - \mathbf{q}_1\|_2. \quad (2)$$

### A. Bistatic InSAR Coverage

Unlike cooperative UAV-based sensing [13], the InSAR coverage is limited to the area in which the beam footprints of  $U_1$  and  $U_2$  overlap, see Figure 2. The coverage problem for UAV-based sensing is challenging because of its near-range nature which causes the swath width to be limited. The usable swath width where the beam footprints of both UAVs overlap can be obtained as follows:

$$S(\mathbf{q}_1, \mathbf{q}_2) = \left[ \min(x_2 + \tan(\theta_{\text{far}})z_2, x_1 + \tan(\theta_{\text{far}})z_1) - \max(x_1 + \tan(\theta_{\text{near}})z_1, x_2 + \tan(\theta_{\text{near}})z_2) \right]^+, \quad (3)$$

where  $\theta_{\text{far}} = \theta_d + \frac{\theta_{3\text{dB}}}{2}$ ,  $\theta_{\text{near}} = \theta_d - \frac{\theta_{3\text{dB}}}{2}$ ,  $\theta_d$  is the depression angle of the SAR antenna, and  $\theta_{3\text{dB}}$  its -3 dB beamwidth in elevation, see Figure 2. Thus, the total area covered by the InSAR radar in time slot  $n$  is approximated<sup>1</sup> as follows:

$$C_N(\mathbf{q}_1, \mathbf{q}_2) = \sum_{n=1}^N S(\mathbf{q}_1, \mathbf{q}_2)v_y[n]\delta_t. \quad (4)$$

Now, let  $r_1$  and  $r_2$  denote the slant range of the radars of  $U_1$  and  $U_2$ , respectively. These slant ranges are given by [4]:

$$r_i(\mathbf{q}_i) = \sqrt{(x_i - x_t)^2 + (z_i)^2}, \forall i \in \{1, 2\}. \quad (5)$$

To maximize the coverage, the master UAV is positioned in the across-track plane such that its SAR antenna beam footprint on the ground is centered at  $x_t$ . Furthermore, we assume  $r_2(\mathbf{q}_2) \leq r_1(\mathbf{q}_1)$  and impose the following condition:

$$x_1 = x_t - z_1 \tan(\theta_d). \quad (6)$$

<sup>1</sup>The approximation is due to the elliptical shape of the beam footprint on the ground and becomes negligible for large  $N$ .

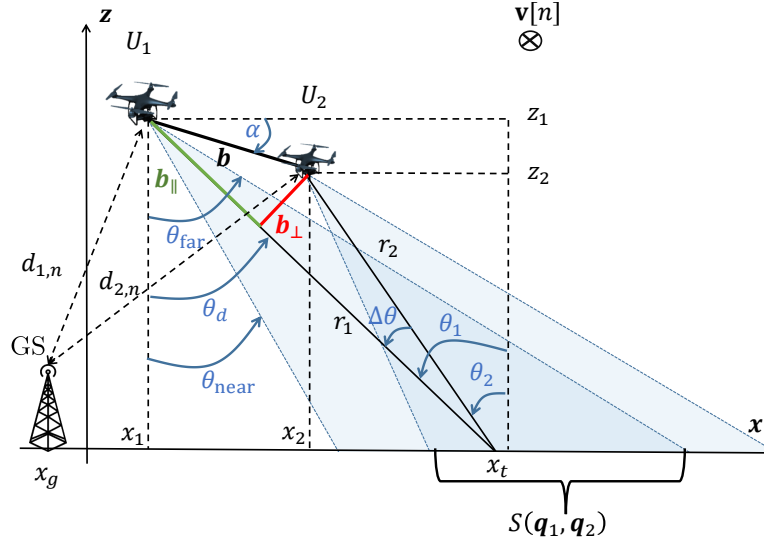


Fig. 2: Illustration of the bistatic UAV formation, denoted by  $\{\mathbf{q}_1, \mathbf{q}_2\}$ , in the across-track plane.

### B. InSAR Performance

Next, we introduce the relevant InSAR sensing performance metrics, namely the coherence and HoA.

1) *InSAR coherence*: Important types of decorrelation that affect InSAR coherence, and thereby InSAR performance, are the signal-to-noise ratio (SNR) decorrelation and baseline decorrelation. In particular, low SNRs in SAR data acquisition result in a loss of coherence between the master and slave SAR images during processing. In time slot  $n$ , the resulting SNR decorrelation is given by [12]:

$$\gamma_{\text{SNR},n}(\mathbf{q}_1, \mathbf{q}_2) = \prod_{i \in \{1,2\}} \frac{1}{\sqrt{1 + \text{SNR}_{i,n}^{-1}(\mathbf{q}_1, \mathbf{q}_2)}}, \forall n, \quad (7)$$

where  $\text{SNR}_{i,n}$  denotes the SNR achieved by  $U_i$  in time slot  $n$ . In particular, the SNR achieved by  $U_1$  is given by [12]:

$$\text{SNR}_{1,n}(\mathbf{q}_1) = \frac{c_n}{r_1^3(\mathbf{q}_1) \sin(\theta_1)}, \forall n, \quad (8)$$

where  $\theta_1$  is the angle that  $U_1$ 's line-of-sight (LOS)<sup>2</sup> has with the vertical and  $c_n = \frac{\sigma_0 P_t G_t G_r \lambda^3 c \tau_p \text{PRF}}{4^4 \pi^3 v_y[n] k_b T_{\text{sys}} B_{\text{Rg}} F L_{\text{atm}} L_{\text{sys}} L_{\text{az}}}$ . Here,  $\sigma_0$  is the normalized backscatter coefficient,  $P_t$  is the radar transmit power,  $G_t$  is the transmit antenna gain,  $G_r$  is the receive antenna gain,  $\lambda$  is the wavelength,  $c$  is the speed of light,  $\tau_p$  is the pulse duration, PRF is the pulse repetition frequency,  $k_b$  is the Boltzmann constant,  $T_{\text{sys}}$  is the receiver temperature,  $B_{\text{Rg}}$  is the bandwidth of the radar pulse,  $F$  is the noise figure, and  $L_{\text{atm}}$ ,  $L_{\text{sys}}$ , and

<sup>2</sup>The radar LOS is defined by the line connecting the UAV with the reference point  $(x_t, 0, 0)$ .

$L_{\text{az}}$ , represent the atmospheric losses, system losses, and azimuth losses, respectively. The SNR achieved by the slave UAV is given by [12]:

$$\text{SNR}_{2,n}(\mathbf{q}_1, \mathbf{q}_2) = \frac{c_n}{r_1^2(\mathbf{q}_1)r_2(\mathbf{q}_2) \sin(\theta_2(\mathbf{q}_2))}, \forall n, \quad (9)$$

where  $\theta_2$  is the angle that  $U_2$ 's LOS has with the vertical.

Another relevant type of decorrelation is the baseline decorrelation. It reflects the loss of coherence caused by the acquisition of the two SAR images in InSAR under different angles. The baseline decorrelation is given by [9]:

$$\gamma_{\text{Rg}}(\mathbf{q}_2) = \frac{(2 + B_p) \sin(\theta_2(\mathbf{q}_2)) - (2 - B_p) \sin(\theta_1)}{B_p (\sin(\theta_1) + \sin(\theta_2(\mathbf{q}_2)))}, \quad (10)$$

where  $B_p = \frac{B_{\text{Rg}}}{f_0}$  is the fractional bandwidth and  $f_0$  is the radar center frequency. It can be shown that a large interferometric baseline results in high baseline decorrelation and, therefore, degrades the coherence.

2) *Height of Ambiguity (HoA)*: The HoA is defined as the height difference which results in a complete  $2\pi$  cycle of the interferometric phase [12]. It is therefore related to the accuracy of the height estimate in the generated digital elevation model (DEM). Similar to the baseline decorrelation, the HoA depends on the UAV formation and is given by [12]:

$$h_{\text{amb}}(\mathbf{q}_1, \mathbf{q}_2) = \frac{\lambda r_1(\mathbf{q}_1) \sin(\theta_1)}{b_{\perp}(\mathbf{q}_1, \mathbf{q}_2)}, \quad (11)$$

where  $b_{\perp}$  is the perpendicular baseline, which is the magnitude of the projection of the baseline vector perpendicular to the slant range, see Figure 2. The perpendicular baseline can be obtained as follows:

$$b_{\perp}(\mathbf{q}_1, \mathbf{q}_2) = b(\mathbf{q}_1, \mathbf{q}_2) \cos(\theta_1 - \alpha(\mathbf{q}_1, \mathbf{q}_2)), \quad (12)$$

where  $\alpha(\mathbf{q}_1, \mathbf{q}_2)$  is the angle between the interferometric baseline and the horizontal plane, see Figure 2. Notice that a large interferometric baseline leads to a small HoA value, and therefore, to a better sensitivity to the ground topography for a given error of the interferometric coherence [5].

### C. Communication Performance

We target real-time offloading of the radar data to a communication ground station (GS), where we adopt frequency-division multiple-access (FDMA) transmission from the master and slave UAVs to the GS. The instantaneous transmit power consumed for communication by the master and slave UAVs is given by  $\mathbf{P}_{\text{com},1} = (P_{\text{com},1}[1], \dots, P_{\text{com},1}[N])^T \in \mathbb{R}^N$  and  $\mathbf{P}_{\text{com},2} = (P_{\text{com},2}[1], \dots, P_{\text{com},2}[N])^T \in \mathbb{R}^N$ , respectively. We denote the location of the GS by  $\mathbf{g} = (x_g, y_g, z_g)^T \in \mathbb{R}^3$  and the distance from  $U_i$  to the GS by  $d_{i,n}(\mathbf{q}_i) = \|\mathbf{q}_i[n] - \mathbf{g}\|_2, \forall i \in \{1, 2\}, \forall n$ . We suppose that both UAVs fly at sufficiently high altitudes to

allow obstacle-free communication with the GS over a LOS link. Thus, based on the free-space path loss model and FDMA, the instantaneous throughput from  $U_i, \forall i \in \{1, 2\}$ , to the GS is given by:

$$R_{i,n}(\mathbf{q}_i, \mathbf{P}_{\text{com},i}) = B_{c,i} \log_2 \left( 1 + \frac{P_{\text{com},i}[n] \gamma}{d_{i,n}^2(\mathbf{q}_i)} \right), \forall n, \quad (13)$$

where  $B_{c,i}$  is the fixed communication bandwidth allocated for  $U_i$  and  $\gamma$  is the reference channel gain<sup>3</sup> divided by the noise variance.

### III. PROBLEM FORMULATION AND SOLUTION

#### A. Problem Formulation

In this paper, we aim to maximize the InSAR coverage by jointly optimizing the UAV formation  $\{\mathbf{q}_1, \mathbf{q}_2\}$  and the communication resources  $\{\mathbf{P}_{\text{com},1}, \mathbf{P}_{\text{com},2}\}$  while satisfying communication and interferometric quality-of-service constraints. To this end, the following optimization problem is formulated:

$$\begin{aligned} \text{(P.1)} : \quad & \max_{\mathbf{q}_1, \mathbf{q}_2, \mathbf{P}_{\text{com},1}, \mathbf{P}_{\text{com},2}} C_N(\mathbf{q}_1, \mathbf{q}_2) \\ \text{s.t.} \quad & \text{C1} : z_{\min} \leq z_i \leq z_{\max}, \forall i \in \{1, 2\}, \\ & \text{C2} : x_1 = x_t - z_1 \tan(\theta_d), \\ & \text{C3} : r_2(\mathbf{q}_2) \leq r_1(\mathbf{q}_1), \\ & \text{C4} : x_2 \leq x_t, \\ & \text{C5} : b(\mathbf{q}_1, \mathbf{q}_2) \geq b_{\min}, \\ & \text{C6} : \gamma_{\text{SNR},n}(\mathbf{q}_1, \mathbf{q}_2) \geq \gamma_{\text{SNR}}^{\min}, \forall n, \\ & \text{C7} : \gamma_{\text{Rg}}(\mathbf{q}_2) \geq \gamma_{\text{Rg}}^{\min}, \\ & \text{C8} : h_{\text{amb}}^{\min} \leq h_{\text{amb}}(\mathbf{q}_1, \mathbf{q}_2) \leq h_{\text{amb}}^{\max}, \\ & \text{C9} : 0 \leq P_{\text{com},i}[n] \leq P_{\text{com}}^{\max}, \forall i \in \{1, 2\}, \forall n, \\ & \text{C10} : R_{i,n}(\mathbf{q}_i, \mathbf{P}_{\text{com},i}) \geq R_{\min,i}, \forall i \in \{1, 2\}, \forall n, \\ & \text{C11} : \sum_{n=1}^N P_{\text{com},i}[n] \delta_t \leq E_{\text{com}}, \forall i \in \{1, 2\}, \forall n. \end{aligned}$$

Note that the InSAR coverage  $C_N$  differs from the cooperative sensing coverage [13]. Constraint C1 define the maximum and minimum allowed flying altitude, denoted by  $z_{\max}$  and  $z_{\min}$ , respectively. Constraints C2

<sup>3</sup>The reference channel gain is the channel power gain at a reference distance of 1 m.

and C3 ensure maximum overlap between the beam footprint of the master drone and the area of interest. Constraint C4 is imposed because a side-looking SAR is assumed. Constraint C5 ensures safe operation, where  $b_{\min}$  is the minimum separation distance of the two drones. Constraints C6 and C7 ensure minimum required coherence thresholds on the sensing SNR and baseline decorrelation, denoted by  $\gamma_{\text{SNR}}^{\min}$  and  $\gamma_{\text{Rg}}^{\min}$ , respectively. Constraint C8 imposes minimum and maximum HoAs denoted by  $h_{\text{amb}}^{\min}$  and  $h_{\text{amb}}^{\max}$ , respectively, that satisfy prescribed DEM requirements [5]. Note that constraints C6, C7, and C8 are specific to InSAR applications and have not been considered in existing UAV-based optimization frameworks. In fact, if the baseline of the UAV formation is too large, the signals are corrupted due to a high baseline decorrelation, while if the baseline is too small, the sensitivity to the ground topology is reduced [6]. Constraint C9 ensures that the communication transmit power is non-negative and does not exceed the maximum allowed level denoted by  $P_{\text{com}}^{\max}$ . Constraint C10 ensures that the achievable throughput of drone  $U_i$  does not fall below the minimum required data rate  $R_{\min,i}$ , which corresponds to an upper bound on the amount of sensing data collected by  $U_i$ . Constraint C11 limits the consumed communication energy to  $E_{\text{com}}$ . Note that some constraints do not depend on time  $n$  as some variables, such as  $x_1$  and  $z_2$ , are optimized but are fixed across time due to the prescribed linear InSAR trajectory imposed by the stripmap mode SAR operation [10].

### B. Solution of the Optimization Problem

Problem (P.1) is non-convex due to its objective function and constraints C3 and C5 – C8, which are non-convex and involve coupled optimization variables  $\mathbf{q}_1$  and  $\mathbf{q}_2$ . In general, it is very challenging to find the globally optimal solution to problem (P.1) and the available optimal algorithms suffer from high time complexity. To strike a balance between performance and complexity, we provide a low-complexity sub-optimal solution for the formulated problem based on alternating optimization (AO). To this end, problem (P.1) is divided into two sub-problems, namely (P.1.a) and (P.1.b).

1) *Slave UAV Optimization:* First, problem (P.1) is solved for fixed  $\{\mathbf{q}_1, \mathbf{P}_{\text{com},1}\}$ . The resulting problem, denoted by sub-problem (P.1.a), is still non-convex and difficult to solve due to its objective function as well as non-convex constraints C5, C7, and C8. Yet, we provide a low-complexity sub-optimal solution based on successive convex approximation (SCA). In a first step, we replace the non-concave objective function with an equivalent concave function.

**Proposition 1.** *Non-concave objective function  $C_N$  can be equivalently replaced by the following concave function:*

$$\tilde{C}(\mathbf{q}_1, \mathbf{q}_2) = \min(x_1 + \tan(\theta_{\text{far}})z_1, x_2 + \tan(\theta_{\text{far}})z_2) - \max(x_1 + \tan(\theta_{\text{near}})z_1, x_2 + \tan(\theta_{\text{near}})z_2). \quad (14)$$



*Proof.* The objective function of problem (P.1), denoted by  $C_N(\mathbf{q}_1, \mathbf{q}_2)$ , can be expressed as  $\delta_t \sum_{n=1}^N v_y[n] \max(0, \tilde{C}(\mathbf{q}_1, \mathbf{q}_2))$ . Therefore, for all  $\mathbf{q}_1$  and  $\mathbf{q}_2$ ,  $C_N(\mathbf{q}_1, \mathbf{q}_2) \geq \delta_t \min_n(v_y[n]) \tilde{C}(\mathbf{q}_1, \mathbf{q}_2)$  holds, meaning that maximizing  $\tilde{C}$  results in maximizing  $C_N$ . Next, we show that the optimal values for  $\tilde{C}$  and  $C_N$  are related by the proportionality constant  $\delta_t \sum_{n=1}^N v_y[n]$ . Let the optimal bistatic formation for problem (P.1) be denoted by  $\{\mathbf{q}_1^*, \mathbf{q}_2^*\}$ . Here, there are two possible outcomes; (i) if  $C_N(\mathbf{q}_1^*, \mathbf{q}_2^*) = 0$ , i.e., there is no feasible solution with non-negative InSAR coverage, then optimizing  $\tilde{C}$  results in reducing the distance along the  $x$ -axis between the ground footprints of the master and slave UAVs, which is not relevant to problem (P.1) as there is no overlap that can be used for interferometry, (ii) if  $C_N(\mathbf{q}_1^*, \mathbf{q}_2^*) > 0$ , then it is easy to note that  $C_N(\mathbf{q}_1^*, \mathbf{q}_2^*) = \delta_t \sum_{n=1}^N v_y[n] \tilde{C}(\mathbf{q}_1^*, \mathbf{q}_2^*)$ . The outcome of (i) and (ii) proves that objective functions  $C_N$  and  $\tilde{C}$  are equivalent.  $\square$

Based on **Proposition 1**, we equivalently maximize objective function  $\tilde{C}$  instead of  $C_N$ . Next, we approximate non-convex constraint C5 with a convex constraint.

**Lemma 1.** *A first-order convex approximation for the concave term  $-b^2(\mathbf{q}_1, \mathbf{q}_2)$  around an arbitrary point  $\mathbf{a} \in \mathbb{R}^2$  and for fixed  $\mathbf{q}_1$  is obtained based on surrogate functions as follows:*

$$g(\mathbf{q}_2) = b^2(\mathbf{q}_1, \mathbf{q}_2) - 2(\mathbf{a} - \mathbf{q}_1)^T(2\mathbf{q}_2 - \mathbf{a} - \mathbf{q}_1). \quad (15)$$

*Proof.* In this proof, we check the first-order conditions for the proposed surrogate function denoted by  $g$ , which are majorization and smoothness [14]. First, let  $f(\mathbf{q}_2) = -b^2(\mathbf{q}_1, \mathbf{q}_2)$ . The gradient of the difference  $g - f$  w.r.t.  $\mathbf{q}_2$  is given by:

$$\nabla_{\mathbf{q}_2}(g - f)(\mathbf{q}_2) = 4(\mathbf{q}_2 - \mathbf{q}_1) - 4(\mathbf{a} - \mathbf{q}_1). \quad (16)$$

Based on (15) and (16), we can easily show that the difference  $g - f$  is non-negative with  $(g - f)(\mathbf{a}) = 0$ , which proves majorization. Second, the difference  $g - f$  is differentiable, its gradient is continuous, and  $\nabla_{\mathbf{q}_2}(g - f)(\mathbf{a}) = 0$ , which proves smoothness and concludes the proof.  $\square$

Based on **Lemma 1**, in the  $j^{\text{th}}$  iteration of the SCA algorithm, constraint C5 can be approximated around point  $\mathbf{q}_2^{(j)} \in \mathbb{R}^2$  by the following convex constraint:

$$\tilde{\text{C5}} : b^2(\mathbf{q}_1, \mathbf{q}_2) - 2(\mathbf{q}_2^{(j)} - \mathbf{q}_1)^T(2\mathbf{q}_2 - \mathbf{q}_2^{(j)} - \mathbf{q}_1) \leq -b_{\min}^2. \quad (17)$$

Next, we use first-order Taylor expansion around point  $\mathbf{q}_2^{(j)} \in \mathbb{R}^2$  to provide a convex approximation for constraint C7:

$$\begin{aligned} \tilde{\text{C7}} : & (x_2 - x_t) - A \sin(\theta_1) r_2(\mathbf{q}_2^{(j)}) - \\ & A \sin(\theta_1) \nabla_{\mathbf{q}_2} r_2(\mathbf{q}_2^{(j)})^T (\mathbf{q}_2 - \mathbf{q}_2^{(j)}) \leq 0, \end{aligned} \quad (18)$$

where  $A = \frac{-\gamma_{\text{Rg}}^{\min} B_p - 2 + B_p}{\gamma_{\text{Rg}}^{\min} B_p - 2 - B_p} \geq 0$ .

**Proposition 2.** *Based on C2 and C3, the perpendicular baseline is independent of  $\mathbf{q}_1$ , and can be rewritten as:*

$$b_{\perp}(\mathbf{q}_2) = \frac{1}{\sqrt{\tan(\theta_1)^2 + 1}} \left| (x_t - x_2) - \tan(\theta_1) z_2 \right|. \quad (19)$$

*Proof.* Please refer to Appendix. A. □

Based on Taylor expansion and **Proposition 2**, non-convex constraint C8 can be approximated around point  $\mathbf{q}_2^{(j)} \in \mathbb{R}^2$  by the following convex constraints:

$$\widetilde{\text{C8a}} : ((x_t - x_2) - \tan(\theta_1) z_2)^2 \leq \frac{a}{(h_{\text{amb}}^{\min})^2}, \quad (20)$$

$$\widetilde{\text{C8b}} : J(\mathbf{q}_2^{(j)}) + \nabla_{\mathbf{q}_2} J(\mathbf{q}_2^{(j)})^T (\mathbf{q}_2 - \mathbf{q}_2^{(j)}) \leq \frac{-a}{(h_{\text{amb}}^{\max})^2}, \quad (21)$$

where  $a = (\tan^2(\theta_1) + 1) \lambda c \tan(\theta_1) z_1$  and  $J(\mathbf{q}_2) = -((x_t - x_2) - \tan(\theta_1) z_2)^2$ . To summarize, sub-problem (P.1.a) is approximated by the following convex optimization problem:

$$\begin{aligned} (\widetilde{\text{P.1.a}}) : \quad & \max_{\mathbf{q}_2, \mathbf{P}_{\text{com},2}} \widetilde{C}(\mathbf{q}_1, \mathbf{q}_2) \\ \text{s.t.} \quad & \text{C1} - \text{C4}, \widetilde{\text{C5}}, \text{C6}, \widetilde{\text{C7}}, \widetilde{\text{C8a}}, \widetilde{\text{C8b}}, \text{C9} - \text{C11}. \end{aligned}$$

The proposed procedure to solve sub-problem (P.1.a) is summarized in **Algorithm 1**, where the convex approximation ( $\widetilde{\text{P.1.a}}$ ) is solved using the Python convex optimization library CVXPY [15]. **Algorithm 1** converges to a local optimum of sub-problem (P.1.a) in polynomial time complexity [16].

---

### Algorithm 1 Successive Convex Approximation for (P.1.a)

---

- 1: For fixed  $\{\mathbf{q}_1, \mathbf{P}_{\text{com},1}\}$ , set initial point  $\{\mathbf{q}_2^{(1)}, \mathbf{P}_{\text{com},2}^{(1)}\}$ , iteration index  $j = 1$ , and error tolerance  $0 < \epsilon \ll 1$ .
  - 2: **repeat**
  - 3: Determine coverage  $\widetilde{C}(\mathbf{q}_1, \mathbf{q}_2)$ ,  $\mathbf{q}_2$ , and  $\mathbf{P}_{\text{com},2}$  by solving ( $\widetilde{\text{P.1.a}}$ ) around point  $\{\mathbf{q}_2^{(j)}, \mathbf{P}_{\text{com},2}^{(j)}\}$ .
  - 4: Set  $j = j + 1$ ,  $\mathbf{q}_2^{(j)} = \mathbf{q}_2$ ,  $\mathbf{P}_{\text{com},2}^{(j)} = \mathbf{P}_{\text{com},2}$ .
  - 5: **until**  $\left| \frac{\widetilde{C}(\mathbf{q}_1, \mathbf{q}_2^{(j)}) - \widetilde{C}(\mathbf{q}_1, \mathbf{q}_2^{(j-1)})}{\widetilde{C}(\mathbf{q}_1, \mathbf{q}_2^{(j)})} \right| \leq \epsilon$
  - 6: **return** solution
- 

2) *Master UAV Optimization:* Next, problem (P.1) is solved for fixed  $\{\mathbf{q}_2, \mathbf{P}_{\text{com},2}\}$ . The resulting problem, denoted by sub-problem (P.1.b), is still non-convex due to the objective function and constraints C5 and C8. Problem (P.1.b) is solved based on SCA, similar to (P.1.a). First, we replace the objective function

$C_N$  with  $\widetilde{C}$  as in (14). Similar to (17), and based on **Lemma 1**, in the  $j^{\text{th}}$  iteration of the SCA algorithm, constraint C5 is approximated around point  $\mathbf{q}_1^{(j)} \in \mathbb{R}^2$ :

$$\widetilde{\widetilde{C5}} : b^2(\mathbf{q}_1, \mathbf{q}_2) - 2(\mathbf{q}_1^{(j)} - \mathbf{q}_2)^T(2\mathbf{q}_1 - \mathbf{q}_1^{(j)} - \mathbf{q}_2) \leq -b_{\min}^2. \quad (22)$$

Based on **Proposition 2** and first-order Taylor expansion, constraint C8 is approximated around point  $\mathbf{q}_1^{(j)} \in \mathbb{R}^2$  by the following convex constraints:

$$\widetilde{\widetilde{C8a}} : r_1(\mathbf{q}_1) \leq \frac{h_{\text{amb}}^{\max} b_{\perp}(\mathbf{q}_2)}{\lambda \sin(\theta_1)}, \quad (23)$$

$$\widetilde{\widetilde{C8b}} : r_1^2(\mathbf{q}_1^{(j)}) + \nabla_{\mathbf{q}_1} r_1(\mathbf{q}_1^{(j)})^T (\mathbf{q}_1 - \mathbf{q}_1^{(j)}) \geq \left( \frac{h_{\text{amb}}^{\min} b_{\perp}(\mathbf{q}_2)}{\lambda \sin(\theta_1)} \right)^2. \quad (24)$$

To summarize, sub-problem (P.1.b) is approximated by the following convex optimization problem:

$$\begin{aligned} (\widetilde{\text{P.1.b}}) : \quad & \max_{\mathbf{q}_1, \mathbf{P}_{\text{com},1}} \quad \widetilde{C}(\mathbf{q}_1, \mathbf{q}_2) \\ \text{s.t.} \quad & \text{C1} - \text{C3}, \widetilde{\widetilde{C5}}, \widetilde{\widetilde{C6}}, \widetilde{\widetilde{C8a}}, \widetilde{\widetilde{C8b}}, \text{C9} - \text{C11}. \end{aligned}$$

Similar to (P.1.a), problem (P.1.b) is solved based on SCA, where the convex approximation  $(\widetilde{\text{P.1.b}})$  is solved using CVXPY [15]. The algorithm converges to a local optimum in polynomial time complexity [16]. As the proposed algorithm is similar to **Algorithm 1**, its detailed steps are omitted.

### C. Solution to Problem (P.1)

To summarize, to solve problem (P.1), we use AO by solving sub-problems (P.1.a) and (P.1.b) iteratively. In **Algorithm 2**, we summarize all the steps of the solution to problem (P.1). Based on [17], **Algorithm 2** converges to a local optimum of problem (P.1) in polynomial time complexity. In practice, this outcome is achieved in just a few iterations.

## IV. SIMULATION RESULTS AND DISCUSSION

In this section, we present simulation results for the proposed UAV formation and resource allocation algorithm. The system parameters are specified in Table I. The proposed solution is compared with the two following benchmark schemes:

**Benchmark scheme 1:** Here, we employ a vertical bistatic formation, i.e., we optimize the  $x$ -position of one of the drones and impose  $x_1 = x_2$  [18]. The remaining optimization variables are determined based on **Algorithm 2**.

**Benchmark scheme 2:** Here, we use equal communication powers, i.e., we optimize  $\mathbf{P}_{\text{com},i}[1]$  and enforce  $\mathbf{P}_{\text{com},i}[n] = \mathbf{P}_{\text{com},i}[n-1]$ ,  $\forall i \in \{1, 2\}$ ,  $\forall n \geq 2$ . The remaining optimization variables are determined by **Algorithm 2**.

---

**Algorithm 2** Alternating Optimization Algorithm
 

---

- 1: Set initial formation  $(\mathbf{q}_1^{(1)}, \mathbf{q}_2^{(1)})$ , initial communication resources  $(\mathbf{P}_{\text{com},1}^{(1)}, \mathbf{P}_{\text{com},2}^{(1)})$ , iteration index  $k = 1$ , and error tolerance  $0 < \epsilon \ll 1$ .
  - 2: **repeat**
  - 3: Determine coverage  $\tilde{C}(\mathbf{q}_1^{(k)}, \mathbf{q}_2)$ ,  $\mathbf{q}_2$ , and  $\mathbf{P}_{\text{com},2}$  by solving (P.1.a) for fixed  $(\mathbf{q}_1^{(k)}, \mathbf{P}_{\text{com},1}^{(k)})$  with initial point  $(\mathbf{q}_2^{(k)}, \mathbf{P}_{\text{com},2}^{(k)})$  using **Algorithm 1**.
  - 4: Set  $k = k + 1$ ,  $\mathbf{q}_2^{(k)} = \mathbf{q}_2$  and  $\mathbf{P}_{\text{com},2}^{(k)} = \mathbf{P}_{\text{com},2}$ .
  - 5: Determine coverage  $\tilde{C}(\mathbf{q}_1, \mathbf{q}_2^{(k)})$ ,  $\mathbf{q}_1$ , and  $\mathbf{P}_{\text{com},1}$  by solving (P.1.b) for fixed  $(\mathbf{q}_2^{(k)}, \mathbf{P}_{\text{com},2}^{(k)})$  with initial point  $(\mathbf{q}_1^{(k-1)}, \mathbf{P}_{\text{com},1}^{(k-1)})$ .
  - 6: Set  $\mathbf{q}_1^{(k)} = \mathbf{q}_1$ , and  $\mathbf{P}_{\text{com},1}^{(k)} = \mathbf{P}_{\text{com},1}$ .
  - 7: **until**  $\left| \frac{\tilde{C}(\mathbf{q}_1^{(k)}, \mathbf{q}_2^{(k)}) - \tilde{C}(\mathbf{q}_1^{(k-1)}, \mathbf{q}_2^{(k-1)})}{\tilde{C}(\mathbf{q}_1^{(k)}, \mathbf{q}_2^{(k)})} \right| \leq \epsilon$
  - 8: **return** solution  $\{\mathbf{q}_1^{(k)}, \mathbf{q}_2^{(k)}, \mathbf{P}_{\text{com},1}^{(k)}, \mathbf{P}_{\text{com},2}^{(k)}\}$
- 

TABLE I: System parameters [5], [9], [11], [12].

Parameter	Value	Parameter	Value	Parameter	value
$z_{\min}$	1 m	$x_g = y_g$	-93 m	$f_0$	2.5 GHz
$z_{\max}$	100 m	$z_g$	2 m	$B_{\text{Rg}}$	3 GHz
$h_{\text{amb}}^{\min}$	0.6 m	$P_{\text{com}}^{\max}$	10 dB	$T_{\text{sys}}$	400 K
$h_{\text{amb}}^{\max}$	2 m	$R_{\min,i}$	1 Mbits	$L_{\text{sys}}$	2 dB
$x_t$	20 m	$E_{\text{com}}$	700 J	$L_{\text{azm}}$	2 dB
$b_{\min}$	2 m	$B_{c,i}$	1 GHz	$L_{\text{atm}}$	0 dB
$\delta_t$	0.5 s	$\gamma$	20 dB	$F$	5 dB
$N$	$10^2$	$\theta_{3\text{dB}}$	$30^\circ$	$\sigma_0$	-5 dBm <sup>2</sup>
$\gamma_{\text{Rg}}^{\min}$	0.8	$\theta_d$	$45^\circ$	$\tau_p \times \text{PRF}$	0.8
$\gamma_{\text{SNR}}^{\min}$	0.8	$v_y$	2 m/s	$G_t$	6 dBi
$P_t$	15 dBm	$\lambda$	0.12 m	$G_r$	6 dBi

Figure 3 illustrates the convergence of the proposed **Algorithm 2**, which solves problem (P.1), as well as that of **Algorithm 1**, which solves sub-problem (P.1.a). For different initial bistatic formations, **Algorithm 2** converges consistently to the same objective function value. Though the convergence rate depend on the initial UAV formation, the optimal value is found in a few iterations for both algorithms.

Figure 4 shows the achieved InSAR coverage versus the maximum UAV communication power,  $P_{\text{com}}^{\max}$ . Benchmark scheme 2, which employs a static communication power allocation, exhibits the lowest performance. Benchmark scheme 1 achieves a higher performance than benchmark scheme 2, due to the

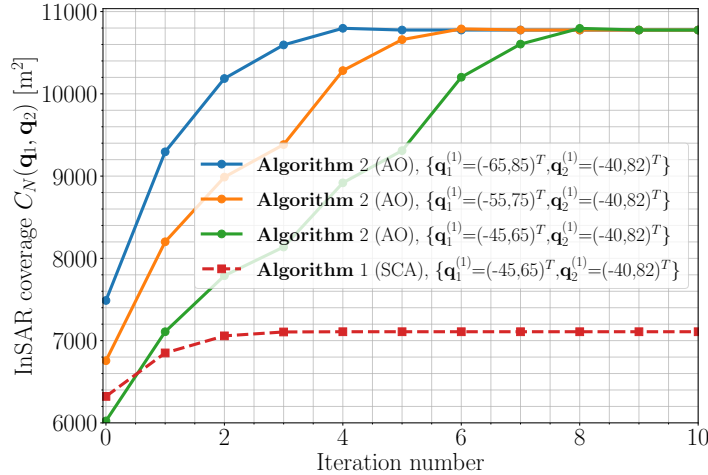


Fig. 3: Convergence of the proposed solution for different initial bistatic UAV formations. The error tolerance is  $\epsilon = 10^{-4}$ .

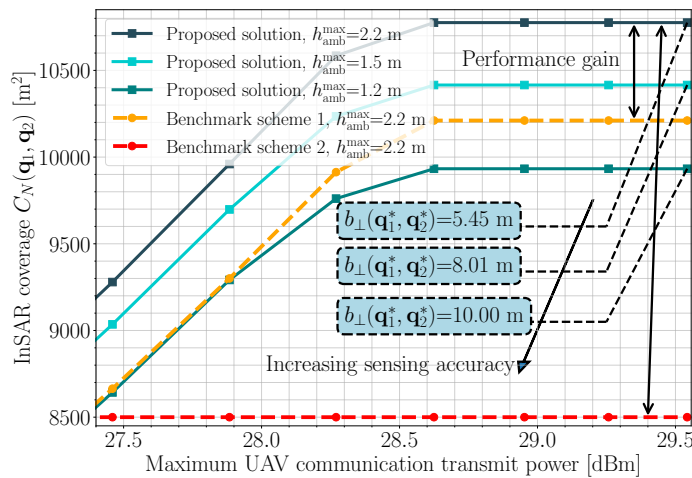


Fig. 4: InSAR total coverage versus maximum UAV communication transmit power,  $P_{com}^{max}$ .

optimization of the communication power allocation, which leads to an enhanced range of the drones. For a maximum HoA of  $h_{amb}^{max} = 2.2$  m, the proposed solution substantially outperforms benchmark schemes 1 and 2 as it jointly optimizes the UAVs formation and the communication resource allocation, with an additionally covered area of more than  $575 \text{ m}^2$  and  $2300 \text{ m}^2$ , respectively. Figure 4 also reveals an interesting InSAR performance trade-off; while a smaller HoA improves the accuracy of the InSAR sensing [4]–[6], it results in a reduced InSAR coverage. This is because a lower HoA necessitates a UAV formation with a larger perpendicular baseline, which in turn leads to an increased offset between the

ground footprints of the master and slave radar systems. For instance, a maximum HoA of 2.2 m requires a perpendicular baseline of only 5.54 m, whereas a maximum HoA of 1.2 m requires a perpendicular baseline of 10 m leading to a loss of 7.48% in total coverage.

## V. CONCLUSION

In this paper, we investigated the UAV joint formation and communication resource allocation optimization for bistatic UAV-based InSAR sensing, where InSAR coverage, interferometric coherence, and HoA were introduced as relevant InSAR sensing performance metrics. A non-convex optimization problem was formulated and solved for the maximization of the bistatic InSAR ground coverage while enforcing the pertinent communication and sensing performance limits. Simulation results confirmed the superior performance of the proposed algorithm compared to two benchmark schemes and emphasized the important role of efficient communication resource allocation for maximum InSAR coverage. We showed that UAV formations with a long perpendicular interferometric baseline, which achieve higher sensing accuracy, result in reduced InSAR coverage. This creates an interesting sensing performance trade-off specific to UAV-based InSAR systems.

## REFERENCES

- [1] M. Mozaffari *et al.*, “A tutorial on UAVs for wireless networks: Applications, challenges, and open problems,” *IEEE Commun. Surv. Tutor.*, vol. 21, no. 3, pp. 2334–2360, 2019.
- [2] G. Pajares, “Overview and current status of remote sensing applications based on unmanned aerial vehicles (UAVs),” *Photogramm. Eng. Remote Sens.*, vol. 81, no. 4, pp. 281–330, 2015.
- [3] A. A. Khuwaja *et al.*, “A survey of channel modeling for UAV communications,” *IEEE Commun. Surv. Tutor.*, vol. 20, no. 4, pp. 2804–2821, 2018.
- [4] R. Bamler and P. Hartl, “Synthetic aperture radar interferometry,” *Inverse Problems*, vol. 14, no. 4, p. R1, 1998.
- [5] M. Martone *et al.*, “Coherence evaluation of TanDEM-X interferometric data,” *ISPRS J. Photogramm. Remote Sens.*, vol. 73, pp. 21–29, 2012.
- [6] G. Krieger *et al.*, “Interferometric synthetic aperture radar (SAR) missions employing formation flying,” *Proc. IEEE*, vol. 98, no. 5, pp. 816–843, 2010.
- [7] K. Meng *et al.*, “UAV-enabled integrated sensing and communication: Opportunities and challenges,” *IEEE Wirel. Commun.*, pp. 1–9, 2023.
- [8] R. Burr *et al.*, “UAV-borne FMCW InSAR for focusing buried objects,” *IEEE Geosci. Remote Sens. Lett.*, vol. 19, pp. 1–5, 2022.
- [9] V. M. Pérez *et al.*, “Towards UAV-based ultra-wideband multi-baseline SAR interferometry,” in *Proc. EuRAD Conf.*, Sep. 2023, to appear.
- [10] D. L. Schuler *et al.*, “Terrain topography measurement using multipass polarimetric synthetic aperture radar data,” *Rad. Sci.*, vol. 35, no. 3, pp. 813–832, 2000.
- [11] M.-A. Lahmeri, W. Ghanem, C. Knill, and R. Schober, “Trajectory and resource optimization for UAV synthetic aperture radar,” in *Proc. IEEE Global Commun. Conf.*, Dec. 2022, pp. 897–903.
- [12] G. Krieger *et al.*, “TanDEM-X: A satellite formation for high-resolution SAR interferometry,” *IEEE Trans. Geosci. Remote Sens.*, vol. 45, no. 11, pp. 3317–3341, 2007.

- [13] X. Chen *et al.*, “Performance of joint sensing-communication cooperative sensing UAV network,” *IEEE Trans. Veh. Technol.*, vol. 69, no. 12, pp. 15 545–15 556, 2020.
- [14] J. Mairal, “Optimization with first-order surrogate functions.” PMLR, 2013, pp. 783–791.
- [15] S. Diamond and S. Boyd, “CVXPY: A python-embedded modeling language for convex optimization,” *J. Mach. Learn. Res.*, vol. 17, no. 83, pp. 1–5, 2016.
- [16] Q. T. Dinh and M. Diehl, “Local convergence of sequential convex programming for nonconvex optimization,” *Recent Adv. Optim. Appl. Eng.*, pp. 93–102, 2010.
- [17] J. C. Bezdek and R. J. Hathaway, “Some notes on alternating optimization,” in *Proc. AFSS Int. Conf. Fuzzy Sys.* Springer, 2002, pp. 288–300.
- [18] Moreira *et al.*, “A drone-borne multiband DInSAR: Results and applications,” in *Proc. IEEE Rad. Conf.*, 2019, pp. 1–6.

## APPENDIX A: PROOF OF PROPOSITION. 2

In this appendix, we derive a simplified expression for the perpendicular baseline. It can be shown that the perpendicular baseline is fixed across the along-track direction, i.e., the  $y$ -direction. Henceforth, we only focus on the across-track plane where the coordinates of an arbitrary point are denoted by  $(x, z)$ . Based on constraints C2 and C3, the perpendicular baseline is the projection of the slave drone  $U_2$  on  $U_1$ 's LOS.  $U_1$ 's LOS, i.e., the line passing through points  $(x_t, 0)$  and  $(x_1, z_1)$ , is characterized by:

$$z = \tan(\theta_1)(x_t - x). \quad (25)$$

The equation of the line perpendicular to (25) passing through point  $(x_2, z_2)$  is given by:

$$z - z_2 = \tan(\theta_1)(x - x_2). \quad (26)$$

Let point  $p$  with coordinates  $(x_p, z_p)$  be the intersection point between lines (25) and (26). The coordinates of  $p$  are derived by solving the system of equations  $\{(25),(26)\}$ , which leads to:

$$x_p = \frac{\tan(\theta_1)}{\tan^2(\theta_1) + 1} \left( \tan(\theta_1)x_2 + \frac{1}{\tan(\theta_1)}x_t - z_2 \right), \quad (27)$$

$$z_p = \frac{1}{\tan^2(\theta_1) + 1} (\tan(\theta_1)(x_t - x_2) + z_2). \quad (28)$$

Using the results in (27) and (28), and after some algebraic manipulations, we can show that the perpendicular baseline, i.e., the distance between points  $(x_p, z_p)$  and  $(x_2, z_2)$ , is given by:

$$b_{\perp}(\mathbf{q}_2) = \frac{1}{\sqrt{\tan^2(\theta_1) + 1}} \left| (x_t - x_2) - \tan(\theta_1)z_2 \right|. \quad (29)$$